

Quantum correlations overcome the photodamage limits of light microscopy

Catxere A. Casacio¹, Lars S. Madsen¹, Alex Terrasson¹,
Muhammad Waleed¹, Kai Barnscheidt², Boris Hage², Michael
A. Taylor³, and Warwick P. Bowen¹

¹ Australian Research Council Centre of Excellence for Engineered Quantum Systems (EQUS), School of Mathematics and Physics, The University of Queensland, St Lucia, QLD 4072, Australia

² Institut für Physik, Universität Rostock, Rostock, Germany

³ Australian Institute for Bioengineering and Nanotechnology, The University of Queensland, St Lucia, QLD 4072, Australia

E-mail: w.bowen@uq.edu.au

Abstract. Light microscopy is a powerful tool to understand the microscopic structure and dynamics of living systems. However, state-of-the-art microscopes use high intensity lasers that cause photodamage, severely disturbing biological processes and functions, and compromising viability^{1,2,3}. This introduces hard limits on their performance, constraining both sensitivity and imaging speed^{1,4,5,6}. Quantum correlations between the photons used in the microscope have been predicted to provide the only means to overcome these limits^{7,8}. Here we demonstrate this, achieving signal-to-noise beyond the photodamage-free capacity of conventional microscopy in a custom-designed ultrahigh efficiency coherent Raman microscope. We use the microscope to image molecular bonds in the interior of a cell with both quantum-enhanced contrast and sub-micron resolution. This allows the observation of nanoscale biological structures that would otherwise be obscured. Coherent Raman microscopes are widely used due to their capacity for extremely selective biomolecular finger-printing in unlabelled specimens^{9,10,11,12}, but photodamage is a roadblock for many applications^{13,14}. By showing that this roadblock can be overcome, and achieving this in a state-of-the-art microscope, our work provides a new path forward, offering the prospect of order-of-magnitude improvements in both sensitivity and imaging speed.

Light microscopy has a long tradition of providing deep insights into the nature of living systems. Recent advances range from super-resolution microscopes that allow the imaging of biomolecules at near atomistic resolution¹⁵, to light-sheet techniques to rapidly explore the dynamics and organisation of organelles in living cells in three-dimensions¹⁶, to adaptive high-speed microscopes for optogenetic control of neural networks^{17,18}. The performance of these microscopes is limited by the stochastic nature of light — that it exists in discrete packets of energy, i.e. photons. Randomness in the times that photons are detected introduces shot-noise, fundamentally constraining sensitivity, resolution and speed⁸. The long-established solution to this problem is to increase the intensity of the illumination light. However, for many advanced microscopes this approach is no longer tenable due to the intrusion of the light on biological processes^{1,14,4}. Light is known to disturb function, structure and growth^{4,14,19}, and is ultimately fatal^{2,14}.

It has been known for many decades that quantum correlations can be used to extract more information per photon used in an optical measurement⁷. This allows the trade-off between signal-to-noise and damage to be broken²⁰. Indeed, for this reason quantum correlations are now used routinely to improve the performance of laser interferometric gravitational wave detectors²¹. The importance of addressing biological photodamage has motivated efforts to apply quantum correlated illumination into microscopy, with recent demonstrations of both quantum-enhanced absorption^{22,23,24,25} and phase-contrast^{26,27} imaging. Quantum correlations have also been used for illumination in infrared spectroscopic imaging²⁸ and optical coherence tomography²⁹. However, all of these experiments used optical intensities more than twelve orders of magnitude lower than those for which biophysical damage typically arises³. Increasing the illumination power to levels relevant for high performance microscopy is a longstanding challenge that has proved difficult due to limitations in methods used to produce quantum correlations, to their fragility once produced, and to the challenge of integration within a precision microscope.

Here we report a microscope that operates safely with signal-to-noise beyond the damage limit of coherent illumination. Light-induced damage is directly observed, imposing a hard bound on intensity, and therefore signal-to-noise. We overcome this bound using quantum-correlated light, demonstrating intracellular imaging with quantum-enhanced contrast and sub-micron resolution. This allows nanoscale biological features to be seen that would have otherwise been buried beneath the shot noise. While the concept is applicable broadly in precision microscopy, we implement it here in a coherent Raman scattering microscope^{13,10,9}. Coherent Raman microscopes probe the vibrational spectra of biomolecules, allowing unlabelled imaging of chemical bonds with exceptionally high specificity — far higher than is possible, for example, using fluorescence^{9,10,11,12}. This provides new capabilities to study a wide range of biosystems and processes, including neurotransmitters³⁰, metabolic processes³¹, nerve degeneration³², neuron membrane potentials³³ and antibiotic response³⁴. However, photodamage places acute constraints on performance^{13,10,14}, presenting a roadblock for powerful prospective applications such as label-free spectrally-multiplexed imaging^{11,12}. State-of-the-art coherent Raman

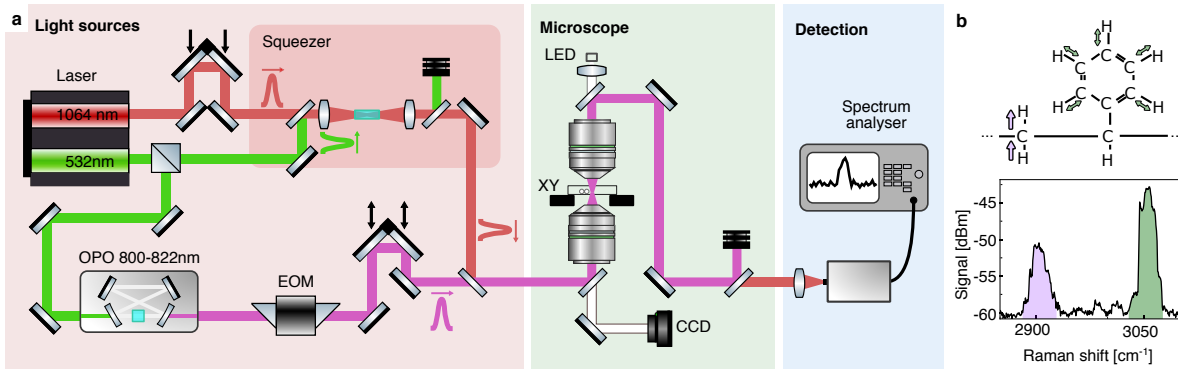


Figure 1. Experimental setup. **a**, Setup schematics. (Red panel) Preparation of the pump beam (purple) via an Optical Parametric Oscillator (OPO) and 20 MHz modulation from an Electro-Optic Modulator (EOM), and Stokes beam (red) which is amplitude squeezed in a periodically poled KTiOPO₄ crystal pumped with 532 nm light. (Green panel) Stimulated Raman scattering is generated in samples at the microscope focus, with raster imaging performed by scanning the sample through the focus. A CCD camera and a light emitting diode (LED) allow simultaneous bright field microscopy. After filtering out the pump, the Stokes beam is detected and the signal processed using a spectrum analyser (blue panel). **b**, Raman spectra measured in a 3 μ m polystyrene bead, showing the CH₂ antisymmetric stretch (purple) and CH aromatic stretch (green) resonances. Taken with 100 kHz spectrum analyser resolution bandwidth (RBW).

microscopes are already limited by shot-noise^{5,6}. The roadblock therefore cannot be overcome through improvements in instrumentation. By using quantum correlations to overcome it, our results remove a fundamental barrier to advances in coherent Raman microscopy and high performance microscopy more broadly.

1. Quantum-compatible coherent Raman microscope

In Raman scattering, a pump photon inelastically scatters from a molecule, exciting a chemical bond vibration and re-emitting a lower frequency Stokes photon. The frequency shift, or *Raman shift*, between pump and Stokes photons corresponds to the vibrational frequency of the bond, providing spectroscopic information about the molecule. However, Raman scattering is inherently weak^{13,12}. Coherent Raman microscopes enhance the process using resonant driving from multiple lasers¹³. The particular coherent Raman microscope constructed here is a stimulated Raman microscope which uses excitation lasers at both pump and Stokes frequencies⁹. The Stokes laser acts to stimulate the Raman process, enhancing the scattering of pump photons.

A schematic of our custom-designed stimulated Raman microscope is shown in Fig. 1a (details in Methods). The Raman scattering rate, and hence signal-to-noise, depends on the product of pump and Stokes laser intensities. Consequently, we use picosecond-pulsed Stokes and pump lasers to reach high peak intensities. Near-infrared wavelengths are chosen to minimise laser absorption and photodamage in biological specimens^{14,8}. To

avoid degradation of quantum correlations we employ custom high numerical aperture water immersion microscope objectives that maintain Stokes transmission $>92\%$, and are also designed to ensure tight focussing of the laser fields and therefore high intensities and spatial resolution. Compared to typical high quality objectives with $\sim 65\%$ efficiency, the high efficiency of our objectives also increases the number of collected Raman scattered photons by 42%, with a commensurate increase in signal strength. At the output of the microscope, the Stokes light is detected on a custom-designed photodetector with very low electronic noise and high bandwidth. Together with previously established laser noise minimisation techniques that shift the Raman signal into modulation sidebands around the Stokes frequency³⁵, this allows shot-noise limited operation with relative intensity noise that is competitive with the best state-of-the-art stimulated Raman microscopes^{35,5} (Methods).

2. Photodamage constrains microscope performance

Before demonstrating that quantum correlations can be used to evade photodamage in Raman microscopy, we systematically explore the shot-noise limited performance of the microscope using dry monodisperse samples of polystyrene beads (see Methods). Fig. 1b shows a typical Raman spectrum, exhibiting several Raman bands. The two strongest bands are the CH₂ antisymmetric stretch and the CH aromatic stretch, illustrated in the figure inset. We focus here on the latter.

To characterise possible photodamage induced by the pump and Stokes lasers we monitor the Raman signal from the CH aromatic stretch band as the pump power is gradually increased over time. At low pump powers, the signal increases as expected. However, at high powers the signal diverges, typically decreasing markedly and decaying over time as shown for example in Fig. 2a. This is a signature of the onset of photodamage. We verify this using bright field imaging which, for this example measurement, shows substantial deformation of the polystyrene bead due to absorptive heating, as well as deformation of an adjacent bead (see Fig. 2a). Measurements on other beads show that other damage modalities also occur, including photoablation due to the high peak pulse intensities (see Methods). The observation of both mean and peak intensity dependent photodamage modalities is an indication that the laser repetition rate and pulse length are well chosen to balance the different classes of photodamage¹⁴.

To determine the photodamage statistics, we repeat the measurement on 110 beads, and record the threshold pump intensity at which the observed signal visibly diverges from damage-free expectations. Fig. 2b plots the distribution, which fits well to a Gaussian with mean power at the sample of 54.6 mW and standard deviation of 7.4 mW. The mean power corresponds to a peak pulse intensity of around $0.9 \text{ kW}/\mu\text{m}^2$ consistent with known thresholds for laser ablation³⁶. The probability of photodamage is highly sensitive to the optical intensity, as shown by the cumulative probability distribution in Fig. 2c. For instance, when using a pump power of 30 mW none of the polystyrene beads exhibited photodamage, while 26% were damaged at 50 mW.

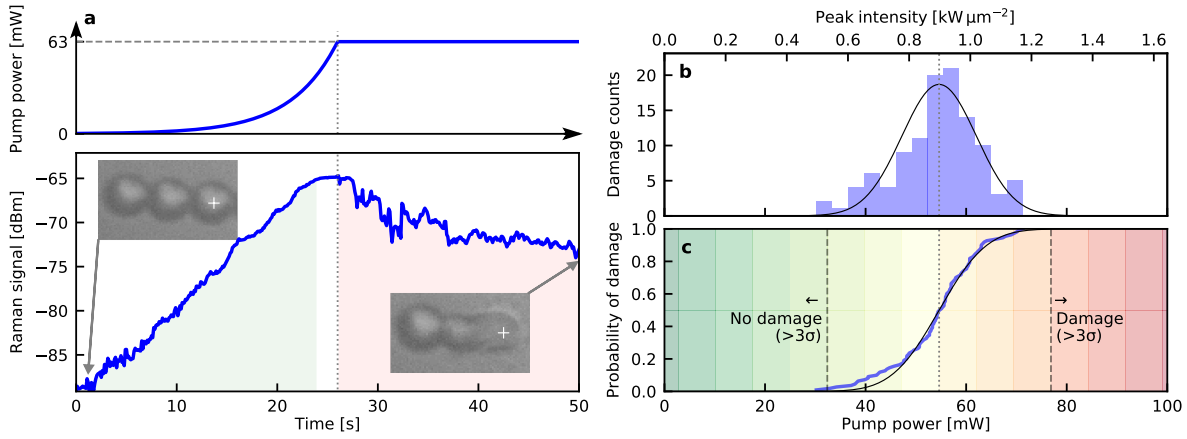


Figure 2. Quantifying photodamage. The Raman signal from a $3\text{ }\mu\text{m}$ polystyrene bead is probed as a function of pump power with a fixed 3 mW Stokes power. **a**, *top*: The pump power is gradually increased until photodamage is observed, in this example occurring at a power at the sample of 63 mW . It is then held fixed. *Bottom*: The Raman signal increases with power prior to photodamage (green) and drops at fixed pump intensity after the particle is damaged (red). Visual inspection (insets) confirms that photodamage has occurred. RBW: 1 kHz . **b,c** Characterization of the photodamage threshold for 110 particles. **b**, Histogram of the pump power at which damage was observed, with Gaussian fit (dashed) of the histogram showing the mean photodamage threshold at 54.6 mW , corresponding to a peak intensity of $0.9\text{ kW}/\mu\text{m}^2$. **c**, Cumulative distribution of the power at which photodamage occurs, with dotted line indicating the mean and each shading bar corresponding to $\pm 1\sigma$ from the mean.

3. Quantum-correlations overcome performance constraints

To increase the signal-to-noise of stimulated Raman microscopy beyond the constraint due to photodamage, we introduce quantum correlations between Stokes photons. The quantum correlations are generated using a home-built optical parametric amplifier that produces bright amplitude squeezed light (see Methods). This allows the measurement noise floor to be reduced beneath the shot-noise. Fig. 3a shows the resulting reduction in noise variance as a function of frequency, with 22% reduction achieved at the frequency of the stimulated Raman modulation sidebands. The bandwidth of quantum-enhancement is greater than 50 MHz , suitable for high speed imaging⁵. Similar quantum correlations – albeit continuous-wave with far lower peak intensity – have been applied in several biophysically-relevant proof-of-principle experiments, demonstrating improvements in sensitivity (e.g. see^{37,38,39}), resolution (e.g. see^{40,41,26}) and fundamental capabilities^{42,28,29}. Quite remarkably, used here they allow Raman scattering to be observed even when less than one photon is scattered on average during the measurement interval, removing what is otherwise a strict constraint on photon budget^{13,4,43}.

To demonstrate quantum-enhanced performance we inject the squeezed Stokes laser into the stimulated Raman microscope while probing the CH aromatic stretch band of a $3\text{ }\mu\text{m}$ polystyrene bead. We then measure the power spectrum of the detected

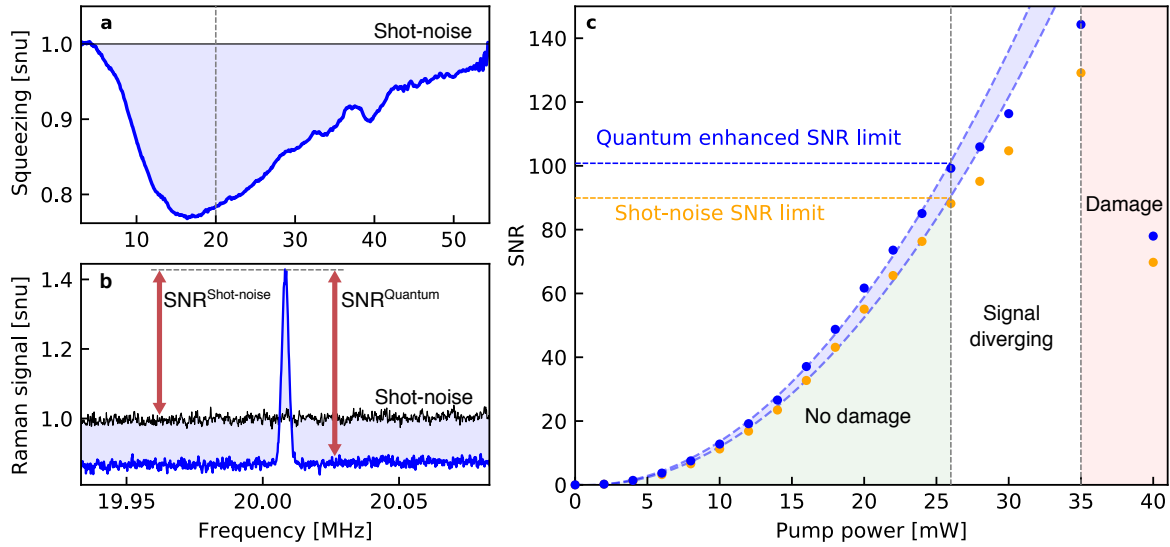


Figure 3. Quantum enhanced stimulated Raman microscopy. **a**, Spectrum of squeezed light detected in the range 1–55 MHz normalised to the shot noise (snu: shot noise units). The maximum squeezing is near the 20 MHz Raman modulation (vertical dashed line). RBW: 1 MHz. **b**, Stimulated Raman signal of a 3 μm polystyrene bead with 3 mW of pump light at the sample, with squeezed light reducing the total measurement noise to 13% below shot noise and thereby improving the signal-to-noise ratio (SNR) by 15%. **c**, SNR for one 3 μm polystyrene particle with increasing pump power. The SNR increases quadratically as expected until 26 mW (green), indicating the particle is undamaged, then rises more slowly, suggestive of some disruption within the particle, and finally drops (red) when the power reaches the threshold for visible damage. Dashed lines are fits to the undamaged SNR, with the blue shading highlighting the increase in quantum enhanced SNR over the shot noise limit. **b&c**, RBW: 3 kHz.

photocurrent. A typical spectrum is shown in Fig. 3b. The peak in the spectrum is the stimulated Raman signal. Losses on transmission through the microscope, pump filters, sample coverslips and polystyrene bead of around 35% degrade the quantum correlations. Never-the-less, the noise floor is still reduced by a factor of 13%, consistent with expectations given the additional loss.

The signal-to-noise is defined as the ratio of the height of the stimulated Raman peak to the power spectrum noise floor. We find that it initially increases quadratically with Raman pump power, as expected for stimulated Raman scattering³⁵. However, as shown for one example in Fig. 3c, the manifestation of photodamage prevents this scaling from continuing indefinitely. When using shot-noise limited light there is a strict maximum in damage-free signal-to-noise, which for the example of Fig. 3c is $\text{SNR}_{\text{max}}^{\text{shot-noise}} = 88$ from a measurement with 3 kHz resolution bandwidth. This corresponds to an estimated minimum detectable concentration of aromatic rings of 20 mM with 1 s of integration (see Methods), comparable to the lower limit achievable for CH bonds in other state-of-the-art stimulated Raman microscopes¹². Quantum correlations enhance the sensitivity, providing a damage-free signal-to-noise of $\text{SNR}_{\text{max}}^{\text{quantum}} = 99$ and a minimum detectable

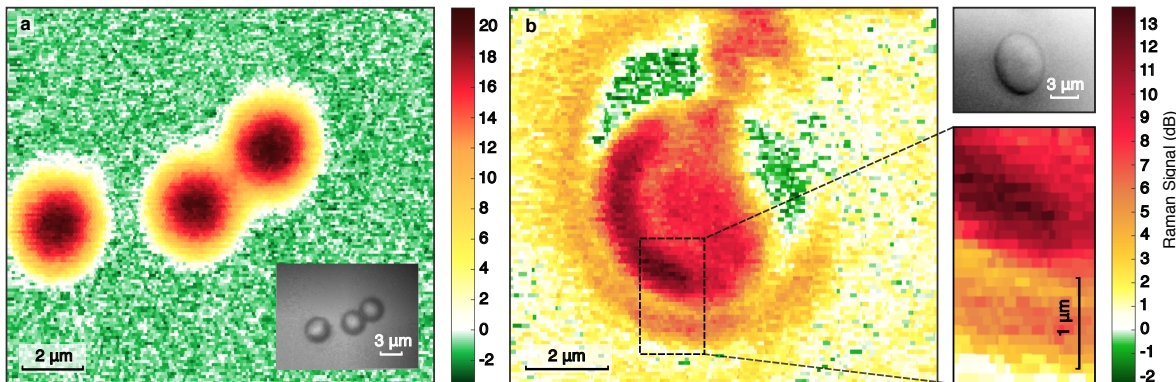


Figure 4. Quantum enhanced imaging. **a**, Image of 3 μm polystyrene beads at a Raman shift of 3055 cm^{-1} obtained with 6 mW of pump power at the sample. The background (coloured green) has no Raman signal, and is limited by measurement noise which is 0.9 dB below shot noise, providing a 23% increase in SNR. **b**, Image of a live yeast cell (*Saccharomyces cerevisiae*) in aqueous buffer at 2845 cm^{-1} Raman shift. The cell nucleus is clearly visible, as well as the faint outline of the cell membrane. A background Raman signal is visible in the buffer outside the cell, possibly due to organic debris, such that squeezing is not visible in the buffer. However a region of intracellular cytosol produced no detectable Raman signal, and here we see noise 0.6 dB below shot noise, indicating that the SNR is increased by 14%. Top inset, cell image in bright-field microscopy. Bottom inset, zoom over the bottom region of the cell. The cell nucleus and membrane are resolvable while being less than a micron apart. Here, the pump power was set to 6 mW, a level that was generally found to be safe for polystyrene (see Fig. 2b&c) and that did not cause visible damage to cells. For both **a&b**, RBW: 1 kHz.

concentration of 19 mM.

We note a parallel demonstration of quantum enhanced sensitivity in stimulated Raman spectroscopy which uses continuous wave excitation sources⁴⁴. Our pulsed excitation and high numerical aperture objectives enable an increase in peak intensity for both pump and Stokes of more than 10^5 , providing an increase in signal-to-noise that is larger again. This is essential for the main conclusions of our work, making the microscope competitive with the state-of-the-art and allowing us to reach the regime where photodamage becomes a constraint. Biological specimens are generally more sensitive to photodamage than polystyrene, and are affected by photochemical intrusion in a variety of ways at intensities lower than those that cause visible damage^{2,14,8}. Therefore, the signal-to-noise enhancement observed in our work is directly relevant to biological imaging applications.

4. Quantum-enhanced imaging

To demonstrate quantum-enhanced imaging, we record the power of the stimulated Raman signal as the microscope sample stage is raster scanned over samples of both dry polystyrene beads and living *Saccharomyces cerevisiae* yeast cells in aqueous solution

(details in Methods). Fig. 4a shows a typical quantum-enhanced image of a collection of 3 μm polystyrene beads, with signal-to-noise enhanced by 23% compared to the shot-noise limit. Fig. 4b shows the equivalent image for a single yeast cell, in this case recorded at a Raman shift of 2841 cm^{-1} to target the CH_2 bonds that are most prevalent in lipids. Here, the microscope benefits fully from the high numerical aperture water immersion objectives, with demonstrated sub-micron spatial resolution (see inset, Fig. 4b). Compared to the bright field microscope image in the inset of Fig. 4b, the Raman image provides significantly more information about the interior structure of the cell. The cell membrane is visible by its faint outline, with a far stronger signal originating from the cell nucleus and a smaller secondary intracellular structure that is likely the vacuole.

In the yeast cell image background Raman scattering is visible outside the cell which could originate from traces of organic material in the aqueous media. However, within the cell there are regions of cytosol in which no Raman scattering is measurable, such that the signal is limited by measurement noise. This allows us to confirm that within the cell the use of squeezed light reduces the noise floor by 12% below shot-noise, thereby improving image contrast. This is particularly useful in subcellular imaging since many features have far-sub-wavelength dimensions and produce a correspondingly small Raman signal. For instance the cell membrane is typically 10 nm thick. In our measurements it generates a Raman signal that ranges in magnitude from 11% below the shot-noise floor to a factor of three above it. Indeed, approximately 11% of the visible membrane generated a signal beneath the shot-noise floor and therefore would not have been observable in a shot-noise limited measurement.

5. Discussion and outlook

Quantum correlations were proposed as a way to overcome the photodamage limits of light microscopy over three decades ago^{7,8}. Our work validates this approach, providing a path to exceed severe constraints on existing high performance microscopes that would otherwise be fundamental^{1,4}. Our results also show that quantum-correlated illumination can both improve microscopes that operate with state-of-the-art performance, and enhance imaging of the interior of a living cell. Our implementation within a coherent Raman microscope provides the capacity for wide impact due to the extremely high specificity and label-free operation such microscopes provide. Coherent Raman microscopes have seen broad applications over the past decade (e.g. see^{13,10,9}). With this progress, both sensitivity and speed are now limited by the constraint that photodamage places on optical intensities. Faster and more sensitive imaging currently requires alternative methods such as fluorescence imaging, for which labels provide far higher cross-sections than are available in label-free Raman scattering. This presents a fundamental barrier for important applications such as video-rate imaging of weak molecular vibrations and label-free spectrally resolved imaging^{12,10}, a barrier that our approach now overcomes.

In absolute terms, the level of improvement achieved here is relatively low. This is

due, in large part, to the relative immaturity of technology capable of generating and detecting bright picosecond squeezed light, together with the relatively low total optical efficiency for squeezed light in our apparatus of approximately 40%. While it may be challenging to achieve high collection efficiency *in vivo*⁵; absorption and scattering of *in vitro* samples is typically very low, as evidenced by the poor contrast of simple bright-field imaging, and therefore should not present a significant constraint. Continuous wave squeezing technology that provides as much as a factor of thirty enhancement in signal-to-noise has been developed to improve the capabilities of gravitational wave detectors⁴⁵. Even allowing for additional optical loss from two high numerical aperture objectives, this suggests that an order-of-magnitude improvement in damage-free signal-to-noise is feasible in future quantum-enhanced coherent Raman microscopes, or equivalently that their frame rate could be increased by the same margin without reducing signal-to-noise. Such an improvement would only otherwise be possible using contrast agents with large Raman scattering cross-sections¹², sacrificing label-free operation. Quantum correlations could also be used to operate with lower light intensities and thereby suppress performance-limiting noise processes such as out-of-focus fluorescence and background scatter⁴³, to improve the single-molecule imaging sensitivity of plasmon-enhanced Raman microscopes⁴⁶, or even to enhance the cross-section of Raman scattering and therefore signal strength⁴⁷.

6. Methods

6.1. Laser sources for stimulated Raman excitation

The Stokes laser is provided by a low noise solid-state pulsed laser with 6 ps pulse length, an 80 MHz repetition rate, and a wavelength of $\lambda_{\text{Stokes}} = 1064$ nm (Coherent, Plecter Duo). Part of the laser output is frequency-doubled to 532 nm and used to pump both the home-built squeezer (described below) and a commercial optical parametric oscillator (OPO; APE, Levante Emerald). The OPO generates a 500 to 700 mW pump laser that is temporally-synchronised and frequency-tunable over a wavelength range from 750 to 900 nm. This provides the capacity to probe Raman shifts over the range 1713–3935 cm⁻¹.

The pulse duration of the laser source was chosen to be comparable to the decay time of molecular vibrations since this maximises the Raman interaction, with molecular decay times typically in the range of a few picoseconds³⁵. The choice of 80 MHz repetition rate is designed to approximately minimise photodamage processes¹⁴. Lower repetition rates lead to higher peak intensity for a given average intensity, thereby increasing the relative contribution of nonlinear damage processes like ablation, while higher repetition rate increases the relative contribution of linear damage for instance due to heating.

Quantum correlations are generated between photons in the Stokes laser by passing the beam through a home-built squeezer, consisting of a second-order nonlinear crystal that is pumped with 532 nm light in a single pass configuration. This forms an optical

parametric amplifier. By controlling the relative phase between the 532 nm pump and Stokes laser it is possible to either amplify or deamplify the Stokes laser. We lock the phase to deamplification. This also deamplifies the amplitude fluctuations, resulting in a bright amplitude squeezed state of light which exhibits pair-wise correlations between photons⁸.

6.2. Microscope design

The microscope is home-made to allow both conventional bright-field imaging and quantum-enhanced stimulated Raman imaging (see Fig. 1a). The microscope frame is home-built in an inverted configuration. Light is both focused and collected in the microscope using two matching water immersion objectives which were custom made by Leica Microsystems. These objectives have custom anti-reflection coating at 1064nm applied in Leica HC-PL-APO63x/1.20W objectives, which ensures ultrahigh Stokes transmission of >92%. To ensure this high transmission is maintained in both dry and aqueous media we under-fill the objectives resulting in an effective NA of 0.9. The objectives have a relatively low ~32% transmission efficiency for pump light. However, the pump intensity is constrained by the photodamage it causes to the sample rather than the laser source (see Fig. 2), and is not sent to the detector (see Fig. 1a) so this attenuation of the pump has no consequence for the achievable signal-to-noise.

The objective focus is controlled using a Mad City Labs Nano-F200S focusing module. Samples are positioned with nanometer scale precision using a Mad City Labs Nano-Bio100 stage, which was used to perform raster scanning in imaging experiments. Samples are simultaneously illuminated with incoherent light from a green LED and imaged using a camera (Allied Vision Manta).

6.3. Reaching the shot-noise limit

Many factors can prevent precision optics experiments from operating at the shot noise floor; most particularly technical laser noise and photodetector electronic noise. Both of these noise sources are especially problematic at low frequencies. To evade low frequency noise, we implement the technique developed in Ref.³⁵ wherein the pump laser is strongly amplitude modulated. This modulates the stimulated Raman process, shifting the detected signal to sidebands around the modulation frequency, and away from the low frequency laser and electronic noise. In our case we use a resonant electro-optic modulator that provides a high depth of modulation at 20.0083 MHz (approximated as 20 MHz elsewhere in the paper).

To minimise electronic noise while still providing a high measurement bandwidth, we custom-build a resonant feedback photodetector, which is designed for resonant detection at frequencies around the modulation sideband frequency. State-of-the-art stimulated Raman microscopes require photodetectors that have high power handling to maximise the useable Stokes laser power and therefore signal-to-noise, high bandwidth to maximise the achievable imaging frame rate, and low electronic noise⁵. As a compromise between

these requirements, we choose a photodiode of 250 μm diameter, with larger diameter allowing better power handling at the cost of slower response and higher electronic noise. When detecting 3 mW of Stokes light, and in the absence of quantum correlations, we find that laser noise dominates electronic noise over a wide frequency band.

To test whether the Stokes laser is shot-noise limited when the optical parametric amplifier is turned off, we measure the variance of its noise at the stimulated Raman modulation frequency as a function of power, detected with the resonant feedback photodetector discussed above and analysed on a spectrum analyser. The result is shown in Fig. 5. Linear scaling is observed, consistent with expectations for a shot-noise limited laser. If the laser were instead limited by technical noise, such as laser relaxation oscillation or spontaneous emission noise, quadratic scaling would be expected. As can be seen by the best-fits to these two possibilities in Fig. 5, it is clear that this is not the case. This verifies that, over the 0–3 mW power range of the measurement, the Stokes laser is shot-noise limited. For a one second integration time τ , we can then estimate the relative intensity noise $\Delta I/I$ of our stimulated Raman microscope. We find $\Delta I/I = (2\hbar c/\eta P \lambda_{\text{Stokes}} \tau)^{1/2} \sim 10^{-8}$, competitive with the best state-of-the-art stimulated Raman microscopes^{35,5}, where $P = 3$ mW is the Stokes power reaching the detector, c the speed of light, and $\eta = 75\%$ the measured quantum efficiency of the photodiode.

6.4. Stimulated Raman scattering

To detect and characterise the stimulated Raman scattering, the Stokes laser is measured on the resonant feedback photodetector and processed with a spectrum analyser. The average Stokes power reaching the detector is kept constant at 3 mW for all experiments, ensuring both shot-noise limited (or squeezed when the optical parametric amplifier is on) performance and large clearance from the electronic noise of the detector. As discussed above, the stimulated Raman process causes the 20 MHz modulation of the pump field to be imprinted on the Stokes field, with the size of the imprinted modulation proportional to the strength of Raman scattering. As such, measurement of the 20 MHz modulation of the Stokes field provides a direct measurement of the Raman gain at the frequency shift between the pump and Stokes fields. The Raman spectrum (Fig. 1b) was measured in polystyrene beads by monitoring this 20 MHz signal while adjusting the OPO to sweep the pump laser wavelength between 800 and 816 nm.

6.5. Characterisation of quantum-enhancement

Throughout the paper, the noise reduction due to quantum correlations was assessed by analysing the noise variance of the photocurrent from the resonant feedback photodetector using a spectrum analyser. The noise was calibrated against shot-noise using the Stokes laser with squeezer switched off as a reference, since this was known to be shot-noise limited (see above). To ensure a fair comparison, the same Stokes power of 3 mW is used at the photodetector with both squeezer on and off. All reported noise floor reductions

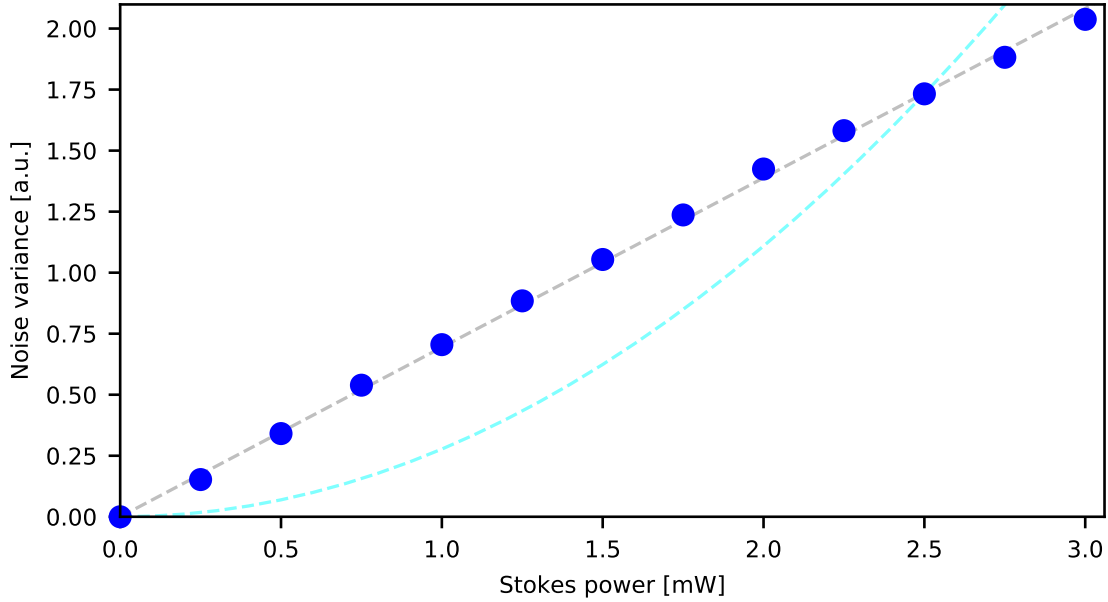


Figure 5. Stokes laser is shot noise limited. Power scaling of Stokes laser noise variance without squeezing, detected with our custom-built resonant feedback stimulated Raman photodetector. The variance is measured at the stimulated Raman modulation sideband frequency of 20.0083 MHz using a spectrum analyser with 1 kHz resolution bandwidth. Dashed grey line: linear fit to the expected scaling for shot noise. Blue dashed curve: quadratic fit expected for technical noise.

are raw: that is, the electronic noise of the photodetector and spectrum analyser is not removed. As such, the measurements represent the actual useful improvement in noise floor that is achieved, rather than the ideal improvement that would be possible if there was no electronic noise.

6.6. Sample preparation

The Raman signal is characterized using polystyrene microspheres. Polystyrene has a relatively simple spectrum with strong Raman bands with Raman shifts in the range of 600 to 3100 cm^{-1} , accessible using our pump and Stokes lasers. The uniform composition and size of the beads allows this Raman spectrum, and the photodamage induced by the measurement, to be accurately and reproducibly characterised. It also allows accurate benchmarking of the performance of the microscope.

Polystyrene bead samples were prepared from dry powder of monodisperse spherical polystyrene beads with 3 μm diameter. These were scattered onto a glass coverslip. Vacuum grease was spread around the edge of the coverslip as a sealant, and a second coverslip pressed on top.

For cellular imaging, dehydrated yeast cells (*Saccharomyces cerevisiae*) were sourced

from a local supermarket, and hydrated in distilled water mixed with sugar (approximately 0.1% by weight) and NaCl salt (approximately 0.1%) to provide sustenance and prevent osmotic shock. The cells were kept in this media for at least an hour to provide time to recover from dehydration. Cells were then transferred into sample chambers by pipetting 15 μL of the cell solution onto a glass coverslip, adding a sealant of vacuum grease around the outer edge of the coverslip, and then pressing a second coverslip on top. The grease forms a seal around the edge while the cell solution fills the approximately 70 μm gap between the coverslips. The sample was then left to rest for an hour before experiments to provide time for the cells to adhere to the surface, which is necessary for raster imaging. The health of the cell culture was verified separately by adding extra sugar and observing the production of carbon dioxide.

6.7. Quantifying optical damage

The damage threshold was characterised for samples of 3 μm polystyrene beads. To find the damage threshold, stimulated Raman signals were recorded in beads as the pump power was gradually increased. The Raman signal generally increases with pump power below the damage threshold, but decays after the onset of damage (with an example shown in Fig. 2a). In all cases the damage was confirmed to have occurred by bright-field imaging. This protocol was repeated for 110 particles with the histogram of recorded damage thresholds shown in Fig. 2b.

Several different damage modalities were observed, as illustrated by the example bright field microscope images in Fig. 6, including deformation due to photoabsorptive heating, ablation due to the high peak intensity of the pump laser, and complete destruction/disintegration.

6.8. Estimation of lower limit to concentration sensitivity

The lower limit to detectable concentration is reached where $\text{SNR}=1$, which we consider for the case of 1 s acquisition time. It is possible to estimate this concentration by extrapolating how the measured SNR changes as the acquisition time changes and the concentration changes. The stimulated Raman signal amplitude scales linearly with concentration C . Since the SNR is linearly proportional to the power of the stimulated Raman signal, it therefore scales quadratically with concentration. Hence, the minimum detectable concentration from a 1 s acquisition time is $C_{\min}(1\text{ s})=C/\text{SNR}(1\text{ s})^{1/2}$. The SNR increases linearly with time so that the SNR for one second acquisition time can be related to $\text{SNR}(\tau)$ for an arbitrary acquisition time τ via $\text{SNR}(1\text{ s})=\text{SNR}(\tau)\times(1\text{ s})/\tau$. We therefore find that the minimum detectable concentration can be found as $C_{\min}(1\text{ s})=C/\text{SNR}(\tau)^{1/2}\times[\tau/(1\text{ s})]^{1/2}$.

Polystyrene is a polymer formed from the monomer styrene, and does not have a well-defined molecular weight or number of aromatic rings. However every aromatic ring corresponds to one styrene monomer. Using the density of polystyrene, 1060 kg/m^3 ,

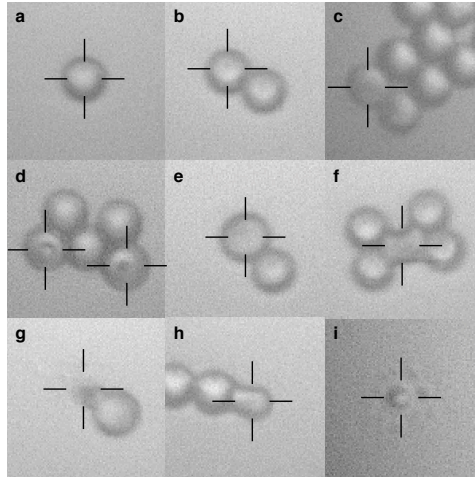


Figure 6. Bright field images of typical photodamage. Examples of the different photodamage modalities that were observed for $3\text{ }\mu\text{m}$ polystyrene beads. **a**, Undamaged bead. **b**, Slight deformation or ablation. **c**, Deformation of target bead and adjacent bead. **d**, Ablation of two beads that were separately exposed. **e**, Deformation. **f**, Significant deformation. **g**, Complete destruction. **h**, Ablation. **i**, Complete disintegration. In each image, the cross-hairs indicate the target bead(s).

and the molecular weight of styrene, 104.15 g/mol, we therefore find the polystyrene concentration to be $C = 10.2\text{ M}$. Note that the unit M corresponds to mol/L.

The damage free shot-noise limited SNR was 88 (Fig. 3c), recorded with 3 kHz resolution bandwidth which corresponds to an effective measurement time of $\tau = 1/3000\text{ s}$. Extrapolating to SNR=1 with 1 Hz resolution bandwidth, the minimum concentration sensitivity is estimated as $C_{\min}(1\text{ s}) = 19.8\text{ mM}$. The quantum enhanced SNR was 99, also recorded with 3 kHz resolution bandwidth. Similarly extrapolating this to SNR=1 provides an estimated minimum concentration sensitivity of $C_{\min}(1\text{ s})18.7\text{ mM}$.

6.9. Imaging

The quantum-enhanced images are formed by recording the stimulated Raman signal on the spectrum analyser while raster scanning the sample in 100 nm steps at a rate of 20 steps per second, returning a 100×100 pixel image in 8.3 minutes. The stage position is recorded throughout the raster scan and is used to assign positions to the measured Raman values. After recording the stimulated Raman signal at each position, the shot noise is also measured at each of the same locations by blocking the pump field, keeping the Stokes power at the detector at 3 mW, and recording shot noise across a similar raster scan. The Raman signal is normalized by dividing by the shot noise level at the same locations, which corrects for any change in signal strength due to attenuation of the detected Stokes field by the sample.

7. References

References

- [1] Bo Li, Chunyan Wu, Mengran Wang, Kriti Charan, and Chris Xu. “An adaptive excitation source for high-speed multiphoton microscopy”. In: *Nature Methods* 17.2 (2020), pp. 163–166.
- [2] Sina Wldchen, Julian Lehmann, Teresa Klein, Sebastian Van De Linde, and Markus Sauer. “Light-induced cell damage in live-cell super-resolution microscopy”. In: *Scientific reports* 5 (2015), p. 15348.
- [3] NP Mauranyapin, LS Madsen, MA Taylor, M Waleed, and WP Bowen. “Evanescent single-molecule biosensing with quantum-limited precision”. In: *Nature Photonics* 11.8 (2017), p. 477.
- [4] Lothar Schermelleh et al. “Super-resolution microscopy demystified”. In: *Nature cell biology* 21.1 (2019), pp. 72–84.
- [5] Brian G Saar et al. “Video-rate molecular imaging in vivo with stimulated Raman scattering”. In: *science* 330.6009 (2010), pp. 1368–1370.
- [6] Christian W Freudiger et al. “Stimulated Raman scattering microscopy with a robust fibre laser source”. In: *Nature photonics* 8.2 (2014), p. 153.
- [7] R. E. Slusher. “Quantum Optics in the '80s”. In: *Opt. Photon. News* 1.12 (1990), pp. 27–30.
- [8] Michael A Taylor and Warwick P Bowen. “Quantum metrology and its application in biology”. In: *Physics Reports* 615 (2016), pp. 1–59.
- [9] Fanghao Hu, Lixue Shi, and Wei Min. “Biological imaging of chemical bonds by stimulated Raman scattering microscopy”. In: *Nature methods* 16.9 (2019), pp. 830–842.
- [10] Ji-Xin Cheng and X Sunney Xie. “Vibrational spectroscopic imaging of living systems: An emerging platform for biology and medicine”. In: *Science* 350.6264 (2015), aaa8870.
- [11] Charles H Camp Jr et al. “High-speed coherent Raman fingerprint imaging of biological tissues”. In: *Nature photonics* 8.8 (2014), p. 627.
- [12] Lu Wei et al. “Super-multiplex vibrational imaging”. In: *Nature* 544.7651 (2017), pp. 465–470.
- [13] Charles H Camp Jr and Marcus T Cicerone. “Chemically sensitive bioimaging with coherent Raman scattering”. In: *Nature photonics* 9.5 (2015), p. 295.
- [14] Yan Fu, Haifeng Wang, Riyi Shi, and Ji-Xin Cheng. “Characterization of photodamage in coherent anti-Stokes Raman scattering microscopy”. In: *Optics express* 14.9 (2006), pp. 3942–3951.
- [15] Yaron M Sigal, Ruobo Zhou, and Xiaowei Zhuang. “Visualizing and discovering cellular structures with super-resolution microscopy”. In: *Science* 361.6405 (2018), pp. 880–887.

- [16] Alex M Valm et al. “Applying systems-level spectral imaging and analysis to reveal the organelle interactome”. In: *Nature* 546.7656 (2017), pp. 162–167.
- [17] KM Naga Srinivas Nadella et al. “Random-access scanning microscopy for 3D imaging in awake behaving animals”. In: *Nature methods* 13.12 (2016), p. 1001.
- [18] Yoav Adam et al. “Voltage imaging and optogenetics reveal behaviour-dependent changes in hippocampal dynamics”. In: *Nature* 569.7756 (2019), pp. 413–417.
- [19] S Waldchen, J Lehmann, T Klein, S van de Linde, and M Sauer. *Light-induced cell damage in live-cell super-resolution microscopy*. *Sci Rep.* 2015; 5: 15348.
- [20] RJ Sewell, M Napolitano, N Behbood, G Colangelo, and MW Mitchell. “Certified quantum non-demolition measurement of a macroscopic material system”. In: *Nature Photonics* 7.7 (2013), p. 517.
- [21] Junaid Aasi et al. “Enhanced sensitivity of the LIGO gravitational wave detector by using squeezed states of light”. In: *Nature Photonics* 7.8 (2013), p. 613.
- [22] Giorgio Brida, Marco Genovese, and I Ruo Berchera. “Experimental realization of sub-shot-noise quantum imaging”. In: *Nature Photonics* 4.4 (2010), p. 227.
- [23] Hugo Defienne, Matthew Reichert, Jason W Fleischer, and Daniele Faccio. “Quantum image distillation”. In: *Science advances* 5.10 (2019), eaax0307.
- [24] J Sabines-Chesterking et al. “Twin-beam sub-shot-noise raster-scanning microscope”. In: *Optics express* 27.21 (2019), pp. 30810–30818.
- [25] Nigam Samantaray, Ivano Ruo-Berchera, Alice Meda, and Marco Genovese. “Realization of the first sub-shot-noise wide field microscope”. In: *Light: Science & Applications* 6.7 (2017), e17005–e17005.
- [26] Yonatan Israel, Shamir Rosen, and Yaron Silberberg. “Supersensitive polarization microscopy using NOON states of light”. In: *Physical review letters* 112.10 (2014), p. 103604.
- [27] Takafumi Ono, Ryo Okamoto, and Shigeki Takeuchi. “An entanglement-enhanced microscope”. In: *Nature communications* 4.1 (2013), pp. 1–7.
- [28] Dmitry A Kalashnikov, Anna V Paterova, Sergei P Kulik, and Leonid A Krivitsky. “Infrared spectroscopy with visible light”. In: *Nature Photonics* 10.2 (2016), p. 98.
- [29] Anna V Paterova, Hongzhi Yang, Chengwu An, Dmitry A Kalashnikov, and Leonid A Krivitsky. “Tunable optical coherence tomography in the infrared range using visible photons”. In: *Quantum Science and Technology* 3.2 (2018), p. 025008.
- [30] Dan Fu, Wenlong Yang, and Xiaoliang Sunney Xie. “Label-free imaging of neurotransmitter acetylcholine at neuromuscular junctions with stimulated Raman scattering”. In: *Journal of the American Chemical Society* 139.2 (2017), pp. 583–586.
- [31] Luyuan Zhang et al. “Spectral tracing of deuterium for imaging glucose metabolism”. In: *Nature biomedical engineering* 3.5 (2019), pp. 402–413.

- [32] Feng Tian et al. “Monitoring peripheral nerve degeneration in ALS by label-free stimulated Raman scattering imaging”. In: *Nature communications* 7.1 (2016), pp. 1–15.
- [33] Bin Liu et al. “Label-free spectroscopic detection of membrane potential using stimulated Raman scattering”. In: *Applied Physics Letters* 106.17 (2015), p. 173704.
- [34] Konstanze T Schiessl et al. “Phenazine production promotes antibiotic tolerance and metabolic heterogeneity in *Pseudomonas aeruginosa* biofilms”. In: *Nature communications* 10.1 (2019), pp. 1–10.
- [35] Christian W Freudiger et al. “Label-free biomedical imaging with high sensitivity by stimulated Raman scattering microscopy”. In: *Science* 322.5909 (2008), pp. 1857–1861.
- [36] Alexander A Oraevsky et al. “Plasma mediated ablation of biological tissues with nanosecond-to-femtosecond laser pulses: relative role of linear and nonlinear absorption”. In: *IEEE journal of selected topics in quantum electronics* 2.4 (1996), pp. 801–809.
- [37] Raphael C Pooser and Benjamin Lawrie. “Plasmonic trace sensing below the photon shot noise limit”. In: *ACS Photonics* 3.1 (2016), pp. 8–13.
- [38] Mohammadjavad Dowran, Ashok Kumar, Benjamin J Lawrie, Raphael C Pooser, and Alberto M Marino. “Quantum-enhanced plasmonic sensing”. In: *Optica* 5.5 (2018), pp. 628–633.
- [39] Michael A Taylor et al. “Biological measurement beyond the quantum limit”. In: *Nature Photonics* 7.3 (2013), p. 229.
- [40] Michael A Taylor et al. “Subdiffraction-limited quantum imaging within a living cell”. In: *Physical Review X* 4.1 (2014), p. 011017.
- [41] Ron Tenne et al. “Super-resolution enhancement by quantum image scanning microscopy”. In: *Nature Photonics* 13.2 (2019), pp. 116–122.
- [42] Nam Mai Phan, Mei Fun Cheng, Dmitri A Bessarab, and Leonid A Krivitsky. “Interaction of fixed number of photons with retinal rod cells”. In: *Physical Review Letters* 112.21 (2014), p. 213601.
- [43] Erich E Hoover and Jeff A Squier. “Advances in multiphoton microscopy technology”. In: *Nature photonics* 7.2 (2013), pp. 93–101.
- [44] RB Andrade et al. “Quantum-Enhanced continuous-wave stimulated Raman spectroscopy”. In: *arXiv preprint arXiv:2002.04674* (2020).
- [45] Henning Vahlbruch, Moritz Mehmet, Karsten Danzmann, and Roman Schnabel. “Detection of 15 dB squeezed states of light and their application for the absolute calibration of photoelectric quantum efficiency”. In: *Physical review letters* 117.11 (2016), p. 110801.
- [46] Cheng Zong et al. “Plasmon-enhanced stimulated Raman scattering microscopy with single-molecule detection sensitivity”. In: *Nature communications* 10.1 (2019), pp. 1–11.

[47] Yoad Michael, Leon Bello, Michael Rosenbluh, and Avi Peer. “Squeezing-enhanced Raman spectroscopy”. In: *npj Quantum Information* 5.1 (2019), pp. 1–9.

8. Acknowledgements

We acknowledge Walter Wasserman for sourcing the yeast cells in trying circumstances. This work was supported primarily by the Air Force Office of Scientific Research (AFOSR) grant FA2386-14-1-4046. It was also supported by the Australian Research Council Centre of Excellence for Engineered Quantum Systems (EQUS, CE170100009). W.P.B. acknowledges the Australian Research Council Future Fellowship, FT140100650. M.A.T. acknowledges the Australian Research Council Discovery Early Career Research Award, DE190100641.